

## Thickness optimization of Al<sub>2</sub>O<sub>3</sub> tunneling layer in CBTS solar cells using SCAPS software

Wafaâ, HENNI

Elaboration and Characterization Physico-Mechanical and Metallurgical of Materials Laboratory (ECP3M), Université Abdelhamid Ibn Badis Mostaganem

RAHAL Wassila Leila

Laboratory of Analysis and Application of Radiation, Faculty of Physics, University of Sciences and Technology of Oran Mohamed Boudiaf, USTO-MB

Djaafar, RACHED

Laboratory of Plasma Physics, Conductive Materials and their Applications (LPPMCA), University of Science and Technology of Oran Mohamed Boudiaf, USTO-MB

Abdelkader, BOUKORTT

Elaboration and Characterization Physico-Mechanical and Metallurgical of Materials Laboratory (ECP3M), Université Abdelhamid Ibn Badis Mostaganem

<https://doi.org/10.5109/7157948>

---

出版情報 : Proceedings of International Exchange and Innovation Conference on Engineering & Sciences (IEICES). 9, pp.59-64, 2023-10-19. 九州大学大学院総合理工学府

バージョン :

権利関係 : Creative Commons Attribution-NonCommercial-NoDerivatives 4.0 International



## Thickness optimization of $\text{Al}_2\text{O}_3$ tunneling layer in CBTS solar cells using SCAPS software

HENNI Wafaa<sup>1\*</sup>, RAHAL Wassila Leila<sup>2,3</sup>, RACHED Djaafar<sup>4</sup>, BOUKORTT Abdelkader<sup>1</sup>

<sup>1</sup>Elaboration and Characterization Physico-Mechanical and Metallurgical of Materials Laboratory (ECP3M), Université Abdelhamid Ibn Badis Mostaganem, Route nationale N°11, kharrouba, 27000, Mostaganem, Algeria

<sup>2</sup>Laboratory of Analysis and Application of Radiation, Faculty of Physics, University of Sciences and Technology of Oran Mohamed Boudiaf, USTO-MB, Algeria

<sup>3</sup>Physics Department, Université Abdelhamid Ibn Badis Mostaganem, Chemin des crêtes, 27000, Mostaganem, Algeria

<sup>4</sup>Laboratory of Plasma Physics, Conductive Materials and their Applications (LPPMCA), University of Science and Technology of Oran Mohamed Boudiaf, USTO-MB, Algeria

\*Corresponding author email: wafaa.henni.etu@univ-mosta.dz

**Abstract:** The purpose of this paper is to explore the possibility for enhancing the performance of CBTS solar cells by incorporating  $\text{Al}_2\text{O}_3$  insulating layer (Eg ~7 eV) between CdS buffer layer and CBTS absorber layer. initially, we performed a comparative analysis between Mo/MoS<sub>2</sub>/CBTS/CdS/ZnO/AZO/Al and Mo/MoS<sub>2</sub>/CBTS/ $\text{Al}_2\text{O}_3$ /CdS/ZnO/AZO/Al using SCAPS-1D. Subsequently, we conducted an investigation into the impact of  $\text{Al}_2\text{O}_3$  thickness on cell performance. Our findings indicate that photovoltaic parameters deteriorate with an increase in  $\text{Al}_2\text{O}_3$  layer thickness, and a thickness of 3nm is sufficient to facilitate the electrons intra-band tunneling. The PCE of the reference cell (without  $\text{Al}_2\text{O}_3$ ) is 6.75%. Upon inserting the alumina layer, the device exhibits a PCE of 11.89% with  $V_{OC}$ ,  $J_{SC}$ , and FF equal to 1.08 V, 15.45 mA/cm<sup>2</sup> and 71.41 % respectively. Although cell efficiency is not fully optimized in this study, we've highlighted the significant utility of  $\text{Al}_2\text{O}_3$  layer in advancing the CBTS solar cells development.

**Keywords:**  $\text{Al}_2\text{O}_3$ ; CBTS; Tunneling, Simulation, SCAPS-1D.

### 1. INTRODUCTION

Solar energy is one of the most widely used forms of renewable energy, which generates electricity using photovoltaic (PV) solar cells [1].

In recent years, thin films based on earth abundant elements such as Cu<sub>2</sub>ZnSnS<sub>4</sub> (CZTS), Cu<sub>2</sub>ZnSnSe<sub>4</sub> (CZTSe), Cu<sub>2</sub>ZnSn(S,Se)<sub>4</sub> (CZTSSe), Cu<sub>2</sub>BaSnS<sub>4</sub> (CBTS), Cu<sub>2</sub>FeSnS<sub>4</sub> (CFTS), and Cu<sub>2</sub>MgSnS<sub>4</sub> (CMgTS) were strongly investigated as PV absorbers [2].

The quaternary Cu<sub>2</sub>BaSnS<sub>4</sub> (CBTS) is a p-type semiconductor with a direct bandgap and a high absorbance coefficient. Ge et al. (2017) realized the highest cell efficiency with a PCE of 2.03% at CBTS/CdS configuration [3]. Adding selenium to the absorber has brought an efficiency of over 5% [4].

The theoretically maximum efficiency of CBTS solar cell is around 25% [5]. However, an unwanted band alignment at the absorber / buffer heterojunction plays the prominent causes of low overall performance and limits  $V_{OC}$  and FF outputs [6] [7].

Several researchers found that using an interlayer at the buffer/absorber heterointerface could be beneficial for cell progress. Erkan et al. (2016) indicated the possibility of enhancing the  $V_{OC}$  by the insertion of the  $\text{Al}_2\text{O}_3$  layer in CZTS solar cells [8]. Ojeda-Durán et al. (2020) demonstrated enhancement in the  $V_{OC}$  and the FF using  $\text{Al}_2\text{O}_3$  ultrathin layers for CZTS/CdS hetero-junctions [9]. The penetration of the carriers through is possible by tunnelling process.

Herein, we performed simulations of Mo/MoS<sub>2</sub>/CBTS/ $\text{Al}_2\text{O}_3$ /CdS/ZnO/AZO/Al solar cell using SCAPS-1D software, then We studied the effect of the  $\text{Al}_2\text{O}_3$  layer thickness on electrical performance, J-V characteristics and tunnelling current density.

### 2. DEVICE STRUCTURE AND SIMULATION

The schematics of the reference device structure (without  $\text{Al}_2\text{O}_3$ ) and the proposed one (with  $\text{Al}_2\text{O}_3$ ) are illustrated in Fig. 1. And Fig.2, respectively.

It consists of MoS<sub>2</sub> BSF layer, CBTS absorber layer,  $\text{Al}_2\text{O}_3$  tunnelling layer, ZnO: Al Transparent Conducting Oxide, and i-ZnO window layer. The Mo back contact and Al front contact.

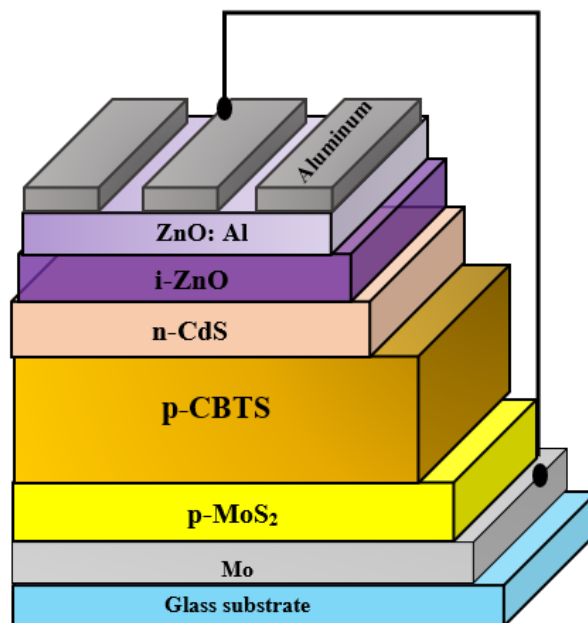


Fig. 1. The schematic representation the reference device.

Table 1. Layer properties [8, 10-25]

	MoS <sub>2</sub>	CBTS	Al <sub>2</sub> O <sub>3</sub>	CdS	ZnO	AZO
W (μm)	0.1	2	0.003	0.02	0.05	0.1
E <sub>g</sub> (eV)	1.7	1.9	7	2.42	3.37	3.6
χ (eV)	4.1	3.6	2.5	4.1	4.5	4.6
ε <sub>r</sub>	13.6	5.4	9.8	9	9	9
N <sub>C</sub> (cm <sup>-3</sup> )	7.5×10 <sup>17</sup>	2.2×10 <sup>18</sup>	1.0×10 <sup>12</sup>	1.8×10 <sup>18</sup>	2.2×10 <sup>18</sup>	2.2×10 <sup>18</sup>
N <sub>V</sub> (cm <sup>-3</sup> )	1.8×10 <sup>18</sup>	1.8×10 <sup>19</sup>	1.0×10 <sup>12</sup>	2.4×10 <sup>19</sup>	1.8×10 <sup>19</sup>	1.8×10 <sup>19</sup>
μ <sub>e</sub> (cm <sup>2</sup> V <sup>-1</sup> s <sup>-1</sup> )	100	30	247	160	150	150
μ <sub>h</sub> (cm <sup>2</sup> V <sup>-1</sup> s <sup>-1</sup> )	150	10	247	50	25	25
N <sub>D</sub> (cm <sup>-3</sup> )	0	0	0	5.0×10 <sup>18</sup>	1.0×10 <sup>17</sup>	1.0×10 <sup>20</sup>
N <sub>A</sub> (cm <sup>-3</sup> )	1.0×10 <sup>16</sup>	5.0×10 <sup>15</sup>	0	0	0	0
N <sub>T</sub> (cm <sup>-3</sup> )	1×10 <sup>14</sup>	1×10 <sup>15</sup>	2.10 <sup>15</sup>	1×10 <sup>17</sup>	1×10 <sup>17</sup>	1×10 <sup>17</sup>

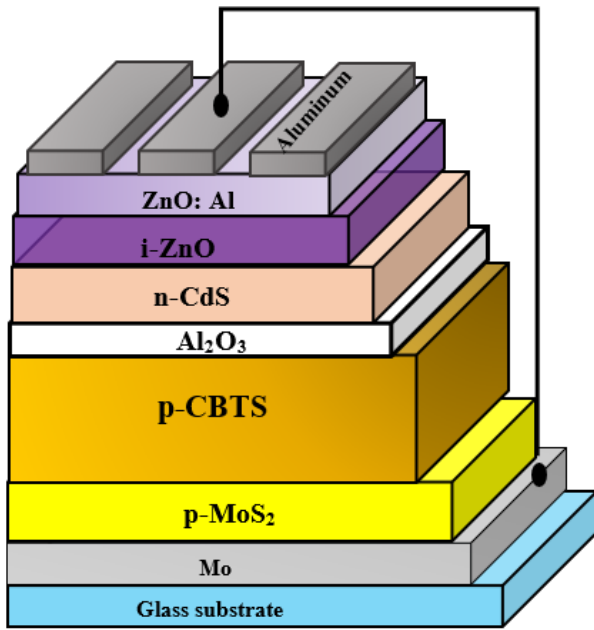


Fig. 2. The schematic of the proposed device.

Here, the simulation is done by the SCAPS-1D. the SCAPS-1D works on three fundamental semiconductor equations which are:

The Poisson's equation:

$$\frac{\partial}{\partial x} \left( \epsilon_0 \epsilon_r \frac{\partial \Psi}{\partial x} \right) = -q \left( p - n + N_D^+ - N_A^- + \frac{\rho_{def}}{q} \right) \quad (1)$$

The continuity equations

$$\frac{dn(t)}{dt} = G_n - R_n - \frac{1}{q} \frac{\partial J_n}{\partial x} \quad (2)$$

$$\frac{dp(t)}{dt} = G_p - R_p - \frac{1}{q} \frac{\partial J_p}{\partial x} \quad (3)$$

Table 2. added defects values

properties	CBTS/CdS [12]	Al <sub>2</sub> O <sub>3</sub> [8]	CBTS/Al <sub>2</sub> O <sub>3</sub>	CdS/Al <sub>2</sub> O <sub>3</sub>
N <sub>T</sub> (cm <sup>-3</sup> )	/	2.10 <sup>15</sup>	/	/
N <sub>it</sub> (cm <sup>-2</sup> )	1.10 <sup>15</sup>	/	1.10 <sup>15</sup>	1.10 <sup>11</sup> [8]
δ <sub>e</sub> (cm <sup>2</sup> )	2.10 <sup>-15</sup>	1.10 <sup>-15</sup>	2.10 <sup>-15</sup>	2.10 <sup>-15</sup>
δ <sub>h</sub> (cm <sup>2</sup> )	2.10 <sup>-15</sup>	1.10 <sup>-13</sup>	2.10 <sup>-15</sup>	2.10 <sup>-15</sup>

The drift-diffusion equations

$$J_n = nq\mu_n E + qD_n \frac{dn}{dx} \quad (4)$$

$$J_p = pq\mu_p E - qD_p \frac{dp}{dx} \quad (5)$$

where  $\Psi$  is the electric potential,  $\epsilon_0$  and  $\epsilon_r$  are the permittivity of the free space and relative, respectively.  $\rho_{def}$  is the defect density,  $N_D^+$  and  $N_A^-$  are the densities of ionized donors and acceptors,  $R$  and  $G$  are the recombination and generation rates of carriers, respectively.  $J_n$  and  $J_p$  are the current densities of electrons and holes.  $D$  and  $\mu$  is the diffusion coefficient and mobility of carriers, respectively.

The parameters of the materials used to simulate the CBTS solar cell are summarized in Table 1.

The interface and Al<sub>2</sub>O<sub>3</sub> layer defects densities are listed in table 2.

The measurements were performed at zero bias, under 300 K, 1.5 AM and light of 1 KW/m<sup>2</sup>.

### 3. RESULTS AND DISCUSSION

We first simulate the cell structure with and without Al<sub>2</sub>O<sub>3</sub> insulator layer, to show how the presence of Al<sub>2</sub>O<sub>3</sub> layer can affect the device performance. The obtained results are summarized in Table 3.

Table 3. Functional parameters of the studied cell with and without Al<sub>2</sub>O<sub>3</sub> layer.

cell	V <sub>oc</sub> (V)	J <sub>sc</sub> (mA/cm <sup>2</sup> )	FF (%)	η (%)
Without Al <sub>2</sub> O <sub>3</sub> layer	0.69	15.09	64.84	6.75
With Al <sub>2</sub> O <sub>3</sub> layer	1.08	15.45	71.41	11.89

According to Table 3, the cell with  $\text{Al}_2\text{O}_3$  layer shows highest photovoltaic parameters ( $V_{OC}$ ,  $J_{SC}$ , FF, and  $\eta$ ). To explain these results, Fig. 3 has been drawn. the band alignment at the CBTS/CdS heterojunction (without  $\text{Al}_2\text{O}_3$  layer) is a cliff.

A cliff-like offset triggers the accumulation of electrons in CdS and increases the recombination process at CBTS/CdS interface between the majority carriers [26], leading to the  $V_{OC}$  degradation.

By inserting  $\text{Al}_2\text{O}_3$  dielectric layer, the built-in electric field at CBTS/ $\text{Al}_2\text{O}_3$ ,  $\text{MoS}_2/\text{CBTS}$  and  $\text{Al}_2\text{O}_3/\text{CdS}$  interfaces increases, indicating higher values of  $V_{OC}$ .

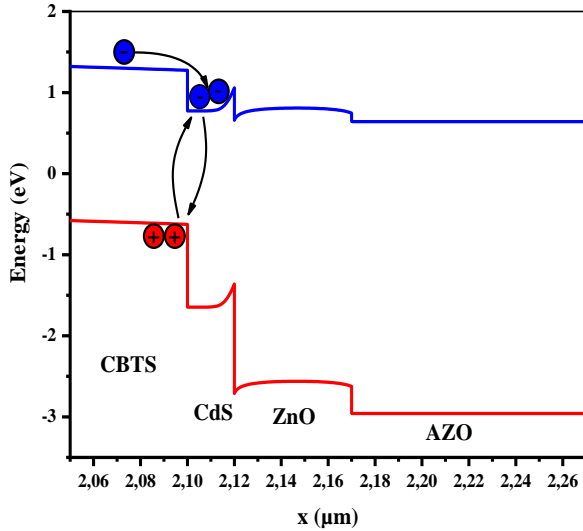


Fig. 3. The energy band diagram of structure without  $\text{Al}_2\text{O}_3$  layer

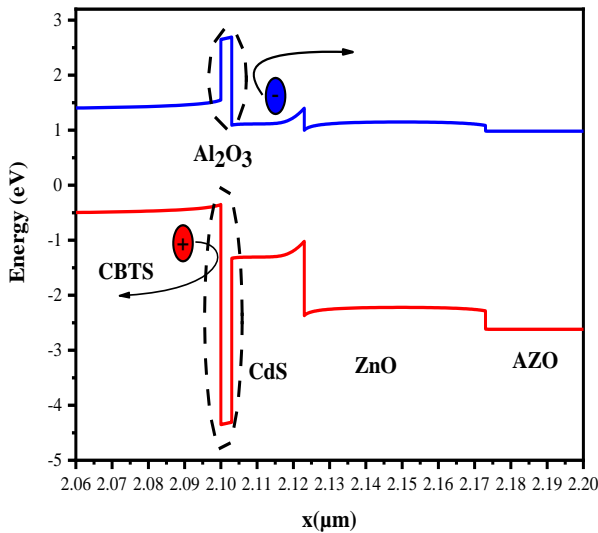


Fig.4 The energy band diagram of device with  $\text{Al}_2\text{O}_3$  layer.

### 3-1 Effect of $\text{Al}_2\text{O}_3$ thickness on PV parameters

In this section, we aim to optimize the  $\text{Al}_2\text{O}_3$  layer thickness, the thickness was changed from 1 nm to 15 nm [9, 27]. The impact of  $\text{Al}_2\text{O}_3$  thickness on J-V curve and the PV parameters is shown in Fig.6 and Fig.7,

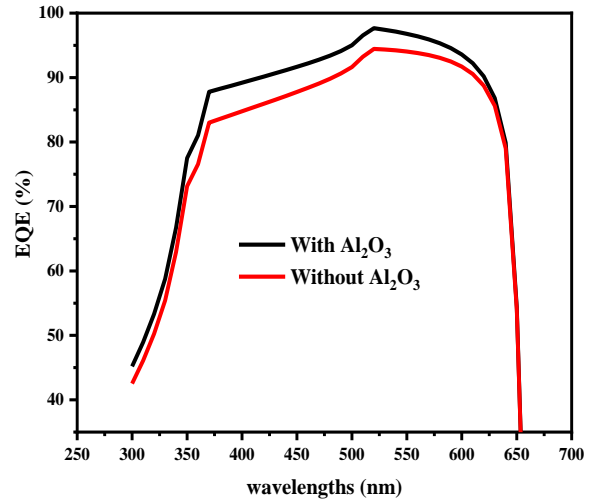


Fig. 5. The EQE vs. Wavelength of both structures (with and without the  $\text{Al}_2\text{O}_3$  layer).

The band diagram of the  $\text{Mo}/\text{MoS}_2/\text{CBTS}/\text{Al}_2\text{O}_3/\text{CdS}/\text{ZnO}/\text{AZO}/\text{Al}$  structure is shown in Fig.4.

By adding the  $\text{Al}_2\text{O}_3$  layer, the structure is characterized by a barrier of 4 eV at valence band at CBTS/  $\text{Al}_2\text{O}_3$  interface and a desired spike-like CBO at CdS/  $\text{Al}_2\text{O}_3$  interface.

The presence of insulator layer is beneficial to block the electrons at front side of the cell and the holes at back side so they cannot recombine with each other, resulting in high carrier collection and this explains why the presence of  $\text{Al}_2\text{O}_3$  improve the EQE values (Fig.5).

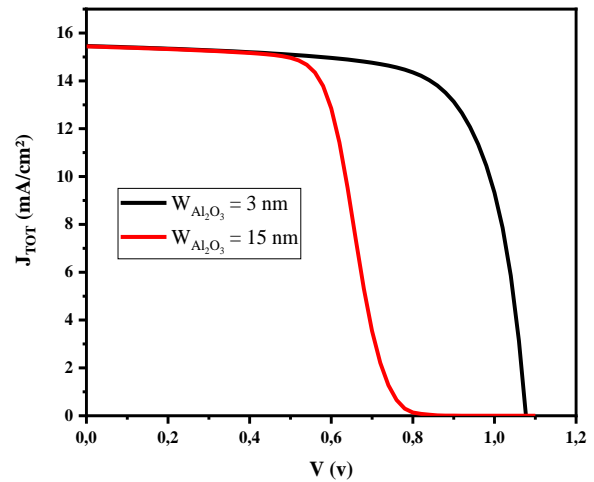
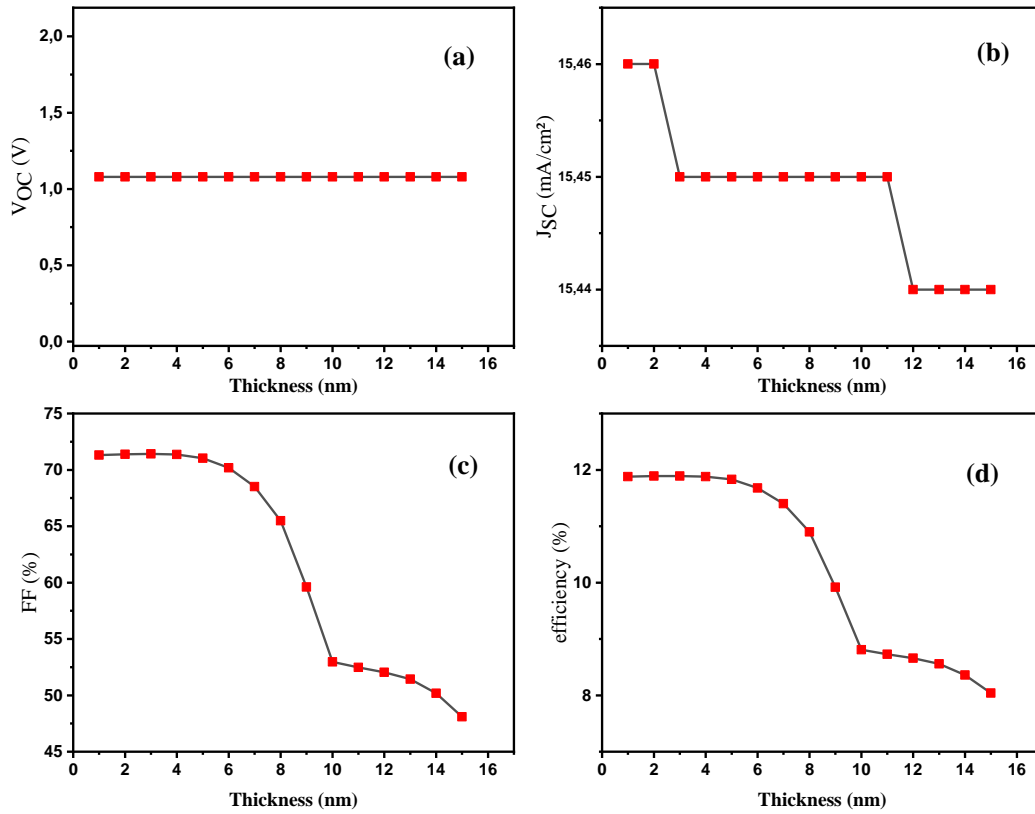


Fig.6 Effect of thickness of  $\text{Al}_2\text{O}_3$  on J-V curve.

respectively. Fig. 7(a) illustrates that the open circuit voltage ( $V_{OC}$ ) is not affected by the  $\text{Al}_2\text{O}_3$  thickness variation and its value remains around 1.08 V.

As shown in Fig. 5(b), the  $J_{SC}$  decreases with the increase of the  $\text{Al}_2\text{O}_3$  layer thickness.


 Fig.7 Effect of  $\text{Al}_2\text{O}_3$  thickness variation on PV parameters.

We observe a similar shape of efficiency and fill factor (FF) curves, implying that the decrease in efficiency is mainly related to the deterioration in FF. The drop in FF with the increase in insulator layer  $\text{Al}_2\text{O}_3$  thickness is due to the increase of tunnelling resistance.

In other words, when the  $\text{Al}_2\text{O}_3$  thickness is increased, the width of the barrier reaches an extent that the photo-generated carriers do not have the energy and time sufficient to cross the barrier.

In Fig.8, we show the influence of the thickness of  $\text{Al}_2\text{O}_3$  on  $J_{Tunnel}$ . It is obvious that the smaller the thickness of  $\text{Al}_2\text{O}_3$ , the higher tunnelling current density delivered ( $J_{Tunnel}$ ).

The optimum thickness of  $\text{Al}_2\text{O}_3$  was observed to be about 3 nm and the PCE is significantly deteriorated from 11.89% to 8.04 % when the thickness increases from 3 to 15 nm.

We found good agreement of the optimum thickness of  $\text{Al}_2\text{O}_3$  with the experimental values that had previously published (Table 4).

#### 4. CONCLUSIONS

In this paper, we have described the effects of  $\text{Al}_2\text{O}_3$  insulator layer on cell performance of CBTS solar cells. To be more precise, we have intended to explain how the insertion of  $\text{Al}_2\text{O}_3$  insulator layer can greatly improve the cell's performance. Furthermore, we have found that a thickness of only 3 nm is enough to allow the transport of photogenerated carriers by tunnelling effect.

Despite the fact that the presence of an  $\text{Al}_2\text{O}_3$  layer enhances device performance, an increase in the thickness of this layer by a few nanometers leads to a significant reduction in FF. our results indicate that an

optimized  $\text{Al}_2\text{O}_3$  has positive impact on the  $V_{OC}$  and the FF and PCE.

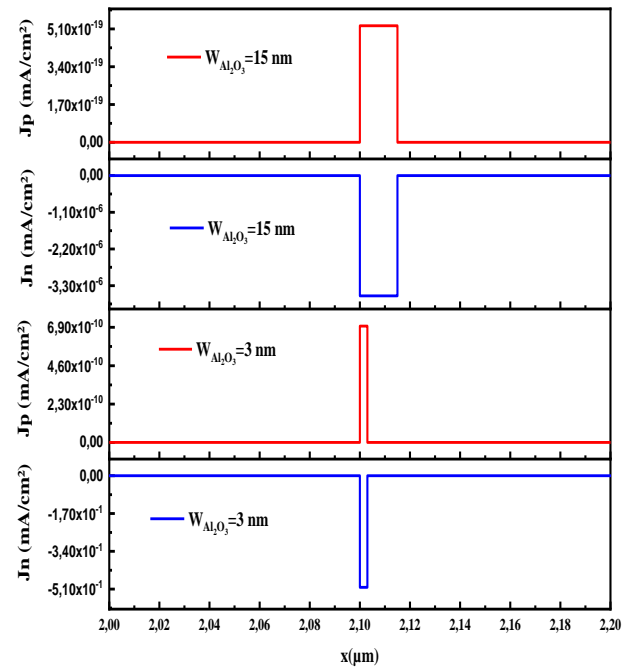

 Fig. 8 Effect of  $\text{Al}_2\text{O}_3$  thickness variation on tunnel current density.

Table 4. comparison of PV parameters of this paper with other reported works.

Structure	V <sub>oc</sub> (V)	J <sub>sc</sub> (mA/cm <sup>2</sup> )	FF (%)	η (%)	Optimal Al <sub>2</sub> O <sub>3</sub> thickness	Ref
Mo/CZTSSe/Al <sub>2</sub> O <sub>3</sub> /CdS/i-ZnO/AZO/Ni-Al	0.336	13.8	29.14	1.35	1 nm	[8]
Mo /CZTS/ CdS/Al <sub>2</sub> O <sub>3</sub> / ITO	0.515	32.1	69.2	11.5	1 nm	[28]
Mo/ Al <sub>2</sub> O <sub>3</sub> / CZTSSe /CdS/AZO/Ni-Al	0.364	35.35	55.46	7.13	5 nm	[29]
Mo/MoS <sub>2</sub> /CZTS/Al <sub>2</sub> O <sub>3</sub> /CdS/ZnO/ITO	0.669	15.7	58.0	6.1	3 nm	[9]
Mo/MoS <sub>2</sub> /CBTS/Al <sub>2</sub> O <sub>3</sub> /CdS/ZnO/AZO/ Al	1.08	15.45	71.41	11.89	3 nm	Our work [30]

## REFERENCES

- [1] Z. Yuhan, H. Farzaneh, Analysis of the different maximum power point tracking strategies in a load-connected photovoltaic system, in Proceedings of International Exchange and Innovation Conference on Engineering & Sciences (IEICES), Interdisciplinary Graduate School of Engineering Sciences, Kyushu University, 2022.
- [2] M.S. Kumar, S.P. Madhusudan, S.K. Batabyal, solution-processed photoactive trigonal Cu<sub>2</sub>BaSnS<sub>4</sub> thin films for efficient solar energy harvesting, *Materials Characterization*, 174(2021). <https://doi.org/10.1016/j.matchar.2021.110988>.
- [3] J. Ge, P. Koirala, C. Grice, P. Roland, Y. Yu, X. Tan, R. J. Ellingson, R. W. Collins, Y. Yan, Oxygenated CdS buffer layers enabling high open-circuit voltages in earth-abundant Cu<sub>2</sub>BaSnS<sub>4</sub> thin-film solar cells. *Adv. Energy Matter*, 7, 16018. (2017). <https://doi.org/10.1002/aenm.201601803>
- [4] D. Shin, T. Zhu, X. Huang, O. Gunawan, V. Blum, D. Mitzi, Earth-Abundant Chalcogenide Photovoltaic Devices with over 5% Efficiency Based on a Cu<sub>2</sub>BaSn(S,Se)<sub>4</sub> Absorber. *Adv. Mater*, 29, 1606945(2017). <https://doi.org/10.1002/adma.201606945>
- [5] W. Shockley, H. Queisser, Detailed balance limit of efficiency of p-n junction solar cells. *J. Appl. Phys*, 32, 510-519(1961). <http://dx.doi.org/10.1063/1.1736034>
- [6] A. Kumar, Efficiency enhancement of CZTS solar cells using structural engineering. *Superlattices and Microstructures*, 153, 106872(2021). <https://doi.org/10.1016/j.spmi.2021.106872>
- [7] T. Song, A. Kanevce, J. Sites, emitter/absorber interface of CdTe solar cells. *Journal of applied physics*, 119, 233104(2016). <https://doi.org/10.1063/1.4953820>
- [8] M. E. Erkan, V. Chawla, M. A. Scarpulla, Reduced defect density at the CZTSSe/CdS interface by atomic layer deposition of Al<sub>2</sub>O<sub>3</sub>. *Journal of Applied Physics*, 119, 194504(2016). <https://doi.org/10.1063/1.4948947>
- [9] E. Ojeda-Durán, K. Monfil-Leyva, J. Andrade-Arvizu, et al. CZTS solar cells and the possibility of increasing VOC using evaporated Al<sub>2</sub>O<sub>3</sub> at the CZTS/CdS interface. *Solar Energy*, 198, 696-703(2020). <https://doi.org/10.1016/j.solener.2020.02.009>
- [10] A. Ghobadi, M. Yousefi, M. Minbashi, A. Ahmadkhan Kordbacheh, A. H. Abdolvahab, N. E. Gorji, Simulating the effect of adding BSF layers on Cu<sub>2</sub>BaSnSSe<sub>3</sub> thin film solar cells. *Optical Materials*, 107, 109927(2020). <https://doi.org/10.1016/j.optmat.2020.109927>
- [11] H. Luo, Y. Zhang, H. Li, Effect of MoS<sub>2</sub> interlayer on performances of copper-barium-tin-sulfur thin film solar cells via theoretical simulation. *Solar Energy*, 223, 384-397(2021). <https://doi.org/10.1016/j.solener.2021.05.074>
- [12] Y. Khattak, F. Baig, H. Toura, S. Beg, B. M. Soucase, Efficiency enhancement of Cu<sub>2</sub>BaSnS<sub>4</sub> experimental thin-film solar cell by device modeling. *J Mater Sci*, 54, 14787-14796(2019). <https://doi.org/10.1007/s10853-019-03942-6>
- [13] G. Gupta, A. Dixit, simulation studies on photovoltaic response of ultrathin CuSb(S/Se)<sub>2</sub> ternary compound semiconductors absorbers –based single junction solar cells. *Int. J. Energy res*, 4, 1-13(2020). <https://doi.org/10.1002/er.5158>
- [14] J. Lin, J. Xu, Y. Yang, Numerical analysis of the effect of MoS<sub>2</sub> interface layers on copper-zinc-tin-sulfur thin film solar cells. *Optik*, 201, 163496(2020). <https://doi.org/10.1016/j.ijleo.2019.163496>
- [15] M. L. Huang, Y. C. Chang, C. H. Chang, T. D. Lin, J. Kwo, T. B. Wu, M. Hong, Energy-band parameters of atomic-layer-deposition Al<sub>2</sub>O<sub>3</sub> / InGaAs heterostructure. *Appl. Phys. Lett*, 89, 012903(2006). <https://doi.org/10.1063/1.2218826>
- [16] M.D. Halls, K. Raghavachari, Atomic Layer Deposition Growth Reactions of Al<sub>2</sub>O<sub>3</sub> on Si(100)-2×1. *The Journal of Physical Chemistry B*, 108, 4058-4062(2004). <https://doi.org/10.1021/jp0378079>
- [17] S. Sharbati, I. Gharibshahian, A.A. Orouji, Designing of Al<sub>x</sub>Ga<sub>1-x</sub>As/CIGS tandem solar cell by analytical model. *Solar Energy*, 188, 1-9(2019). <https://doi.org/10.1016/j.solener.2019.05.074>



- [18] A. Basak, U. P. Singh, Numerical modelling and analysis of earth abundant Sb<sub>2</sub>S<sub>3</sub> and Sb<sub>2</sub>Se<sub>3</sub> based solar cells using SCAPS-1D. *Solar Energy Materials and Solar Cells*, 230, 111184(2021). <https://doi.org/10.1016/j.solmat.2021.111184>
- [19] N. Beyrami, M. Saadat, Z. A. Sohbatazadeh, modeling study on utilizing In<sub>2</sub>S<sub>3</sub> as a buffer layer in CIGS-based solar cells. *J Comput Electron* 21, 1329–1337 (2022). <https://doi.org/10.1007/s10825-022-01927-4>
- [20] S.R.I. Biplab, M.H. Ali, M.M.A. Moon, et al. Performance enhancement of CIGS-based solar cells by incorporating an ultrathin BaSi<sub>2</sub> BSF layer. *J Comput Electron* 19, 342–352 (2020). <https://doi.org/10.1007/s10825-019-01433-0>
- [21] B. Bibi, B. Farhadi, W., ur Rahman, et al. A novel design of CTZS/Si tandem solar cell: a numerical approach. *J Comput Electron* 20, 1769–1778 (2021). <https://doi.org/10.1007/s10825-021-01733-4>
- [22] W. Henni, W.L. Rahal, D. Rached, Path Toward High-Efficiency CZTS Solar Cells with Buffer Layer Optimization. *Acta Phys. Pol. A* 142, 445(2022). <http://doi.org/10.12693/APhysPolA.142.445>
- [23] F. A. Jhuma, M. J. Rashid, I. Sharnali, Numerical Simulation of Highly Efficient Lead-free MAgel<sub>3</sub> Based Perovskite Solar Cell for Various ETL and HTL Layers, in Proceedings of International Exchange and Innovation Conference on Engineering & Sciences (IEICES), Interdisciplinary Graduate School of Engineering Sciences, Kyushu University, 2022.
- [24] M. Minbashi, A. Ghobadi, M. H. Ehsani, H. Rezagholipour Dizaji, and N. Memarian. "Simulation of high efficiency SnS-based solar cells with SCAPS." *solar energy* 176 (2018): 520-525.
- [25] I.E. Tinedert, A. Saadoune, I. Bouchama, M.A. Saeed, 2020. Numerical modelling and optimization of CdS/CdTe solar cell with incorporation of Cu<sub>2</sub>O HT-EBL layer. *Optical Materials*, 106, p.109970.
- [26] S. E. Maklavani, S. Mohammadnejad, Enhancing the open-circuit voltage and efficiency of CZTS thin-film solar cells via band-offset engineering. *Opt Quant Electron*, 52, 1-22(2020). <https://doi.org/10.1007/s11082-019-2180-6>
- [27] N. M. Terlinden, G. Dingemans, M.C. Sanden, W. M. Kessels, Role of field-effect on c-Si surface passivation by ultrathin (2–20 nm) atomic layer deposited Al<sub>2</sub>O<sub>3</sub>. *Appl. Phys. Lett*, 96,112101(2010).<https://doi.org/10.1063/1.3334729>
- [28] Y.S Lee, T. Gershon, T.K. Todorov, et al. Atomic layer deposited aluminum oxide for interface passivation of Cu<sub>2</sub>ZnSn (S, Se) 4 thin-film solar cells. *Advanced Energy Materials*, 6(12), 1600198(2016). <https://doi.org/10.1002/aenm.201600198>
- [29] J. Kim, S. Park, S. Ryu, J. Oh, B. Shin, Improving the open-circuit voltage of Cu<sub>2</sub>ZnSnSe<sub>4</sub> thin film solar cells via interface passivation. *Progress in Photovoltaics: Research and Applications*, 25(4), 308-317(2017). <https://doi.org/10.1002/pip.2864>
- [30] W. Henni, W.L. Rahal, D. Rached, A. Boukortt, Effect of introducing Al<sub>2</sub>O<sub>3</sub> as a tunnelling layer into p-CBTS/n-CdS heterojunction solar cells. *J Comput Electron* 22, 897–905 (2023). <https://doi.org/10.1007/s10825-023-02031-x>